Biomass and Bioenergy 172 (2023) 106772

Contents lists available at ScienceDirect

Biomass and Bioenergy

journal homepage: www.elsevier.com/locate/biombioe

Production, characteristics and use of magnetic biochar nanocomposites as sorbents

A.A. Burbano [a,b,c], G. Gascó [c,*], F. Horst [a], V. Lassalle [a], A. Méndez [b]

[a] INQUISUR, Departamento de Química, Universidad Nacional Del Sur (UNS)-CONICET, Av. Alem 1253, 8000, Bahía Blanca, Argentina
[b] Department of Geological and Mining Engineering, Universidad Politécnica de Madrid, 28040, Madrid, Spain
[c] Department of Agricultural Production, Universidad Politécnica de Madrid, Ciudad Universitaria, 28040, Madrid, Spain

ARTICLE INFO

Keywords:
Biochar
Hydrothermal carbonization
Nanoparticles
Nanocomposite
Malachite green

ABSTRACT

Magnetic biochar nanocomposites were obtained by in-situ co-precipitation of magnetite nanoparticles into carbon-based matrixes prepared by three different procedures: i) pyrolysis of sunflower husk (MBC_{SFH}); ii) hydrothermal carbonization (HTC) of sunflower husk (MHC_{SFH}) and iii) HTC of orange juice residue (MHC_{OR}). Besides, two magnetic carbon nanocomposites were obtained in the same way using commercial activated carbon (MAC) and charcoal (MCC). All the materials were widely characterized by elemental analysis, N_2 isotherms, FTIR, and Z potential and used in the sorption of malachite green (MG) from water. Kinetic fitting was done using pseudo-first-order and pseudo-second-order kinetic models, where it was found that experimental data fitted well with the second-order kinetic model. MHC_{SFH} and MHC_{OR} exhibited the maximum removal efficiencies (77.00% and 82.18%) compared to their corresponding carbon precursors (63.32% and 34.29%). The post-sorption characterization of MHC_{OR} indicates electrostatic interactions, electron sharing, and π-π interactions and pore filling are the principal interactions between sorbent and MG. In addition to the synthesis and characterization of magnetic biochar nanocomposites, this research demonstrated the capacity of sorbents materials for pollutants removal.

1. Introduction

The discharge of organic and inorganic pollutants into water sources has been increasing due to anthropogenic activities, especially those related to industry and agriculture. These pollutants are sometimes persistent or pseudo-persistent, which could alter the ecosystem and even cause severe damage to human organisms [1]. One well-known group is synthetic dyes that have been employed since 1856 with the accidental discovery of Mauve. Since then, they have been used in many industries, including textile, leather, plastic, paper, food, and pharmaceutical [2]. These pollutants are responsible for the increase of chemical oxygen demand (COD), biochemical oxygen demand (BOD), toxicity at low concentrations, high dissolved oxygen consumption in water bodies, and reduced light capacity penetration in aquatic systems [3–6].

Malachite green (MG) is a cationic triarylmethane dye commercialized as chloride and oxalate. It is commonly used in aquaculture as an antiprotozoal and antifungal [7,8]. However, due to its high solubility and stability, it can cause effects on the reproductive and immune systems and has genotoxic and carcinogenic properties [9–13]. Although the US Food and Drug Administration (FDA) has disapproved of its use, it is still being implemented in many countries due to its low cost, availability, and efficacy [14,15]. There are many physical, biological, and chemical treatments to remove dyes such as MG from water bodies, including coagulation, flocculation, ultrafiltration, biodegradation, sorption, and advanced oxidation processes [16–18]. Sorption has gained considerable attention since it appears as a low-cost, feasible, versatile, and easy operational treatment [19,20]. The nature of the sorption mechanism between sorbent and sorbate depends on the sorbent's chemical composition, porous properties, and chemical parameters such as pKa and Kow of the sorbate. Chemical bonds or physical interactions, including hydrogen bonds, electrostatic, van der Waals, London dispersion, and hydrophobic interactions, may occur [21,22].

Several sorbents are available, standing out commercial activated carbon that is the most widely used sorbent due to its high sorption capacity. Nevertheless, its high cost of preparation, including expensive feedstocks, high temperatures, and subsequent chemical or physical activation treatments, has caused the development of alternative low-cost sorbents [23–27]. Thermochemical treatment of lignocellulosic

* Corresponding author.
E-mail address: gabriel.gasco@upm.es (G. Gascó).

https://doi.org/10.1016/j.biombioe.2023.106772
Received 19 July 2022; Received in revised form 13 February 2023; Accepted 27 March 2023

wastes, including slow pyrolysis, fast pyrolysis, gasification, torrefaction, and hydrothermal carbonization, can transform them into added-value biochars [28–32]. The valorization of lignocellulosic wastes into biochar implements the concept of circular economy and the carbon-negative processes [33]. Tsai et al. [34] prepared mesoporous biochar derived from rice husk (obtained from hydrothermal alkali carbonization) for malachite green's efficient sorption from wastewater, obtaining special removal rates of almost 100% at pH 6. Experiments in natural water (stream and seawater) were carried out also in this study, obtaining high percent removal efficiencies up to >96%, which indicates the affinity of malachite green molecules for the active sites of the biochar. Furthermore, Leng et al. [35] prepared biochar from rice husk (obtained from liquefaction) as a malachite green sorbent. The experimental results showed that the biochar is rich in oxygen-containing functional groups involved in malachite green's sorption mechanism and achieved sorption capacitates between 32.5 and 67.6 mg L^{-1}, considering that the temperature of the synthetic procedure was conducted at 260 °C. Recent studies have added inorganic or organic compounds to the carbonaceous matrixes to convert them into hybrid materials allowing them to act as bifunctional ones [36–41]. For example, magnetite nanoparticles could provide magnetic properties to the carbonaceous material. That would be useful for the recovery of the materials post-sorption, for instance, in water remediation procedures utilizing a simple magnet. Yi et al. (2021) prepared magnetic biochar from rice straw to sorb crystal violet [42]. The material showed efficient removals percentages of 97%. The kinetics fitting (by pseudo-first and pseudo-second-order models) and the characterization results (by XPS, XRD, Raman analysis, and FTIR) suggested that the main sorption mechanisms are $\pi - \pi$, H-bonding, and electrostatic interactions. Moreover, Huang et al. [43] synthesized magnetic biochars (from rice straw (M-RHB) and sewage sludge (M-SSB)) that were compared with the non-magnetic biochars (RHB and SSB) for the sorption of Cd^{2+}. After magnetization of the biochars, the sorption capacities diminished from 58.65 (RSB) and 7.22 mg L^{-1} (SSB) to 42.48 (M-RSB) and 4.64 mg L^{-1} (M-SSB). The main Cd^{2+} sorption mechanisms proposed were precipitation, complexation, and cation exchange. Another research study used empty fruit bunch, a residue from palm oil of the industry of Malaysia, to synthesize magnetic biochar by microwave heating technique [44]. The obtained material had a high surface area of 890 $m^2 g^{-1}$ and was demonstrated to have highly efficient for methylene blue removal of about 99.9% from aqueous solution.

There is controversy about the rate-limiting mechanism of sorption in magnetic carbon nanocomposites, which is directly affected by the physicochemical properties of the sorbate and the sorbent. At the same time, the sorbent is influenced by the utilized feedstock and the presence of iron oxide nanoparticles which can modify the sorption capacity of carbonaceous materials. For this reason, the main objective of the present research is to study the removal of MG employing magnetic biochar nanocomposites obtained by pyrolysis and hydrothermal carbonization of biomass wastes. Two magnetic carbon nanocomposites were obtained in the same way using commercials activated carbon and charcoal in terms of comparing the adsorption performance with those carbonaceous materials obtained from biomass residue. It is essential to highlight that few or any works were found in the literature that analyzes the adsorption capacity of not only the carbonaceous matrix but also the magnetic nanocomposites of them. Besides, a great variety of different sources of residue biomass was employed for the synthesis. Moreover, this work analyzes the obtained carbon materials by two different methodologies; hydrothermal and pyrolysis. An exhaustive characterization of all materials was conducted and the adsorption efficiency for malachite green dye was examined in all adsorbents.

2. Materials and methods

2.1. Materials

Malachite oxalate green ($C_{52}H_{54}N_4O_{12}$, C.I. 42000, M = 927.02 g mol^{-1}) was purchased from PanReac Química SA (CAS number 2437-29-8, Spain). Table 1 summarizes their main chemical properties. Iron (II) sulfate heptahydrate ($FeSO_4{\cdot}7H_2O$, M = 278.02 g mol^{-1} was from Labkem (CAS number 7782-63-0, Spain). Iron (III) chloride 6-hydrate ($FeCl_3{\cdot}6H_2O$, M = 270.32 g mol^{-1}) was purchased from PanReac AppliChem (CAS number 10025-77-1, Spain). Sodium hydroxide (NaOH, M = 40 g mol^{-1}) was supplied by Merck (CAS number 1310-73-2, Darmstadt-Germany). Commercial activated carbon was purchased from PanReac ITW companies (CAS number 7440-44-0, Spain). Charcoal was obtained from Ibecosol (Spain).

2.2. Preparation of carbonaceous sorbents

Commercial activated carbon (CAC), charcoal (CC), biochar obtained from sunflower husk (BC_{SFH}), hydrochar obtained from sunflower husk (HC_{SFH}), and hydrochar obtained from the orange residue (HC_{OR}) were synthesized by hydrothermal carbonization and pyrolysis methods. CAC was utilized as supplied. CC was crushed and sieved until a homogeneous grain size (lower than 100 μm). BC_{SFH} was prepared using sunflower husk (SFH) as the feedstock and pyrolysis as the thermochemical treatment. In this respect, a certain amount of SFH was placed into the crucibles and transferred to the muffle utilizing a heating rate of 18 °C min^{-1} until 700 °C. The final pyrolysis temperature was maintained for 2.5 h in an inert atmosphere. Besides, HC_{SFH} was obtained using sunflower husk and HTC. The experimental procedures were done following the steps published previously [45]. HC_{OR} was prepared by using orange residue as the feedstock and HTC. The orange residue was mixed with distilled water and transferred into a reactor at 240 °C for 6 h.

2.3. Synthesis of magnetic carbonaceous sorbents

Magnetic activated carbon (MAC), magnetic charcoal (MCC), magnetic biochar from sunflower husk (MBC_{SFH}), magnetic hydrochar from the orange residue (MHC_{OR}), and magnetic hydrochar from sunflower husk (MHC_{SFH}) were prepared by the in-situ co-precipitation method [46]. First, each carbonaceous precursor was placed into a beaker with 250 mL of Fe^{3+} and Fe^{2+} solution with a 2:1 M ratio until a homogeneous dispersion was obtained. Then, NaOH 5 M was added dropwise using a burette (there must be a base excess as seen in reaction 1).

$$2Fe^{3+}{}_{(aq)} + Fe^{2+}{}_{(aq)} + 8OH^-_{(aq)} \rightarrow Fe_3O_4{}_{(aq)} + 4H_2O{}_{(aq)} \quad (1)$$

As NaOH is added to the solution that contains the mixture of Fe^{3+}/Fe^{2+}/carbon matrix, magnetite nanoparticles follow formation, nucleation, and growth into the carbon matrix. This procedure was followed by Santhosh et al. [47] with certain modifications. The whole synthesis can be observed in Fig. 1.

2.4. Characterization of magnetic carbonaceous sorbents

Carbonaceous sorbents (CAC, CC, BC_{SFH}, HC_{OR}, and HC_{SFH}) and the corresponding magnetic carbonaceous sorbents (MAC, MCC, MBC_{SFH}, MHC_{OR}, and MHC_{SFH}) derived from them were characterized as follows: the elemental composition (H, C, N, and S) was analyzed by dry combustion using a LECO CHNS 932 Analyzer (SCAI-Malaga University, Spain). Ash content was calculated by combustion of samples at 850 °C in a Heron furnace. Oxygen was obtained by difference as 100%-(%C+%H+%N+%S+%Ash). Atomic ratios H/C, and O/C, were also calculated. The chemical bonds and functional groups were analyzed and compared using Fourier Transform Infrared Spectroscopy with an equipment

Table 1
Elemental analysis of the carbonaceous and magnetic carbonaceous sorbents.

Sample	C (%)	H (%)	N (%)	S (%)	O[a] (%)	H/C	O/C	Ash (%)	pH	Eh (mV)
CAC	85.71	0.88	0.00	0.00	12.41	0.12	0.11	1.00	8.03	453
CC	80.21	3.12	0.92	0.00	0.81	0.47	0.01	14.94	8.31	355
HC_{SFH}	67.02	5.41	0.45	0.00	26.92	0.97	0.30	0.20	4.30	467
BC_{SFH}	84.71	0.82	0.42	0.10	8.45	0.11	0.07	5.49	10.48	280
HC_{OR}	60.81	4.75	1.09	0.13	27.23	0.94	0.34	5.99	5.57	476
MAC	47.24	0.46	0.00	0.09	2.37	0.11	0.04	49.83	8.50	320
MCC	35.74	1.55	0.00	0.00	9.15	0.52	0.19	53.54	9.50	331
MHC_{SFH}	28.55	2.65	1.13	0.00	15.35	1.11	0.40	52.32	7.09	453
MHC_{OR}	25.89	2.28	0.31	0.16	15.01	1.06	0.43	56.34	9.30	360
MBC_{SFH}	40.45	0.58	0.04	0.09	8.19	0.17	0.15	50.62	8.52	415

[a] Calculated by difference.

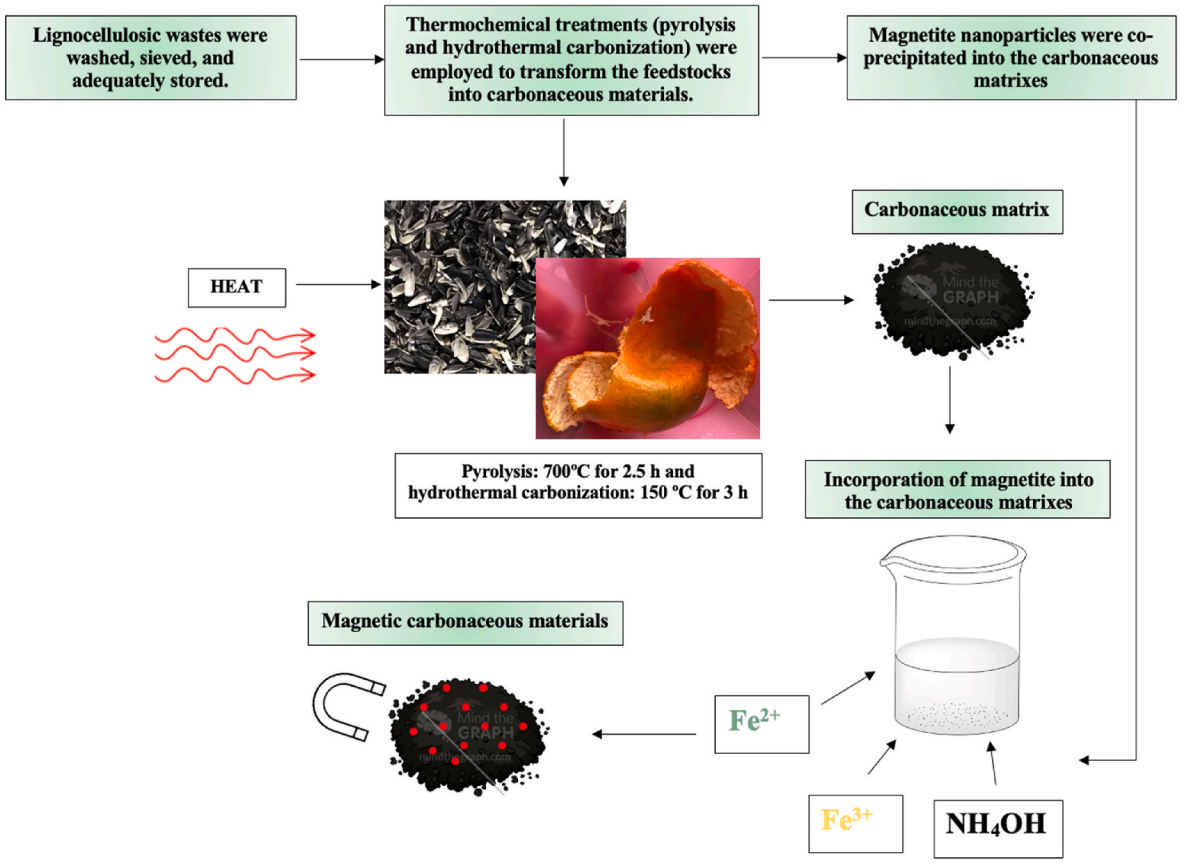

Fig. 1. Synthesis of magnetic carbonaceous solids employing lignocellulosic residues which suffered a heating treatment that converted them into carbon-rich materials which were employed as matrixes for magnetite nanoparticles deposition.

6800FV Jasco Analitica. pH and Eh (mV) of carbonaceous and magnetic carbonaceous sorbents were determined on aqueous solutions at a concentration of 4 g L^{-1} of a carbon sample in distilled water solution using a Crison micro pH 2000 and a pH 60 DHS, respectively. BET surface area (S_{BET}) and porous properties were estimated by N_2 adsorption-desorption using a Porosimetry System ASAP 2420 Micromeritics. Zeta potential was determined by Nano-ZS90X, Malvern, UK, and the average hydrodynamic diameter was obtained by Dynamic Light Scattering (DLS). Zeta potential measurement was carried out by adjusting the ionic strength utilizing NaCl 0.001 M. Besides, the porous structure of the carbonaceous matrixes was analyzed by Scanning Electron Microscope (SEM LEO EVO 40 XVP) employing secondary electrons.

2.5. Batch sorption experiments

Sorption kinetics of malachite green using all the materials synthesized (CAC, CC, BC_{SFH}, HC_{OR}, HC_{SFH}, MAC, MCC, MBC_{SFH}, MHC_{OR}, and MHC_{SFH}) was carried out in a water bath shaker using 250 mL of a 30 ppm solution of the dye and 250 mg of each sorbent (chemical parameters can be observed in the supplementary material). Sorption kinetics was performed at room temperature and fixed initial pH value under constant stirring. It is important to note that the initial pH value of each material's suspension was different (see supplementary material). Aliquots were taken at different intervals of time, i.e., 10, 20, 30, 50, 70, and 120 min. The final dye concentration of each aliquot was analyzed at 618 nm wavelength using a UV–Vis (Zuzi spectrophotometer 4201/50). The amount of dye sorbed at the equilibrium qe (mg g^{-1}) was calculated by the following equation

$$qe = \frac{(Ci - Ce)V}{m} \quad (2)$$

Where Ci, Ce, V, and m are the initial concentration (mg L^{-1}), the concentration at the equilibrium (mg L^{-1}), the batch volume (L), and the mass (g) of the sorbent, respectively.

2.6. Kinetic models

Sorption analysis has been completed using kinetic models, which allow understanding of sorption pathways, probable mechanisms involved, and possible rate-limiting steps. To complete this analysis regarding the possible nature of the interactions between the sorbent and the sorbate (i.e., physisorption or chemisorption), experimental data were fitted into kinetic models such as pseudo-first and pseudo-second-order.

2.6.1. Pseudo-first-order (PFO)

It is also known as the Largengren model. It assumes that the rate-limiting involves the diffusion process and that the sorption kinetic depends only on the sorbate concentration. This model is controlled by physisorption phenomena. PFO equation is defined as follows:

$$\frac{dqt}{qt} = k1\ (qe - qt) \quad (3)$$

After integration, the linearized form of PFO obtained is

$$ln\ (qe - qt) = ln\ qe - k1t \quad (4)$$

Where qt is the sorption capacity at the time t (mg g^{-1}), qe is the sorption capacity at the equilibrium (mg g^{-1}), and k_1 is the rate constant for the pseudo-first order model (min^{-1}).

2.6.2. Pseudo-second-order (PSO)

It assumes that the rate-limiting step is mediated by chemisorption, which is related to sharing electrons between the surface of the sorbent and the sorbate. PSO equation is expressed as:

$$\frac{dqt}{dt} = k2\ (qe - qt)^2 \quad (5)$$

After the equation is integrated and considering the boundary conditions, the PFO equation is defined as:

$$\frac{1}{qt} = \frac{1}{k2qe^2} + \frac{1}{qet} \quad (6)$$

Where qt is the sorption capacity at the time t (mg g^{-1}), qe is the sorption

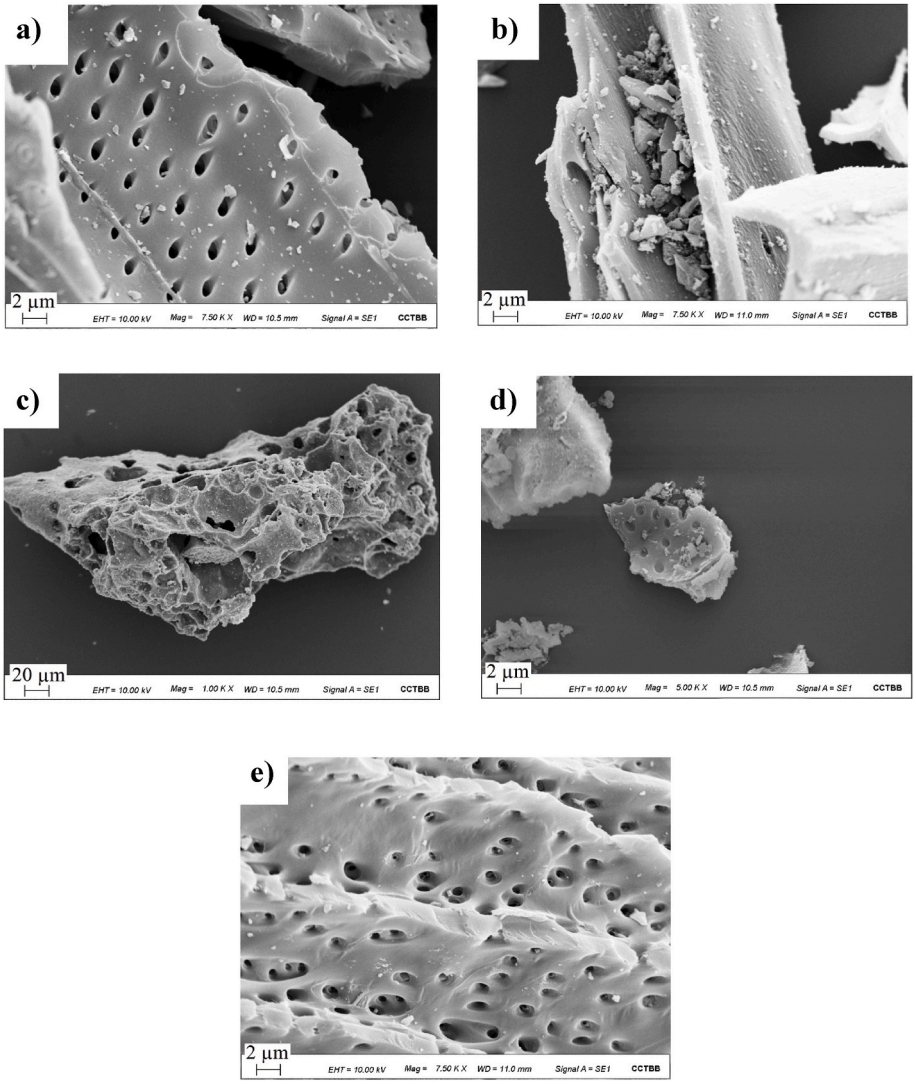

Fig. 2. SEM micrographs a) CAC, b) CC, c) $H_{OR,}$ d) HC_{SFH}, and e) BC_{SFH}.

capacity at the equilibrium (mg g^{-1}), and k_2 is the rate constant for the pseudo-second-order model (g mg^{-1} min^{-1}).

3. Results and discussion

3.1. Characterization of carbonaceous sorbents

3.1.1. Morphology

Fig. 2 shows SEM micrographs of carbonaceous matrixes. As illustrated, CAC and BC_{SFH} have the most well-defined and well-developed porous structures due to the high temperatures employed in their preparation. Volatile matter and tar are removed inside the pores at a specific temperature, thus enhancing the porous structure [48].

Contrary to the above-mentioned, CC does not possess pores related to the operational parameters employed in its preparation, such as feedstock, temperature, and the absence of an activating agent. On the other hand, HC_{OR} and HC_{SFH} have pores; however, they are not well-formed and non-homogeneous in the carbonaceous matrixes.

3.1.2. Elemental composition

Elemental analysis results (shown in Table 1) provide helpful information about the changes in %C, %H, %N, %S, and %O when transforming lignocellulosic biomass into carbon-rich materials through thermochemical processes (pyrolysis or hydrothermal carbonization). The analysis of the non-magnetic carbonaceous materials shows that CAC, CC, and BC_{SFH} present the highest carbon contents (>80%), while the two hydrochars, HC_{SFH} and HC_{OR}, present values of 67.08 and 60.81 wt%, respectively. Previous works have shown that carbonaceous sorbents obtained via pyrolysis have greater carbon content than those obtained from hydrothermal carbonization due to the mild conditions used during HTC [49,50]. Both hydrochars HC_{SFH} and HC_{OR} show high oxygen content (26.92 and 27.23 wt%, respectively). These results are consistent with previous research where hydrochars (compared to biochars) show more oxygen-containing functional groups [51,52]. CAC offers a high oxygen content compared to CC and BC_{SFH} due to the activation process to prepare commercial activated carbon. For the magnetic carbonaceous sorbents, the presence of magnetite nanoparticles increased the ash content, decreasing the carbon percentage. It is important to note that the carbon matrix seems to be modified during the co-precipitation process of magnetite nanoparticles, depending on the carbonaceous material characteristics. The oxygen content of MAC was lower than that of CAC, indicating the loss of oxygenated functional groups, whereas, in the case of CC, the treatment of the carbonaceous material in basic solution during the co-precipitation process of magnetite nanoparticles increased the oxygen content from 0.81% for CC to 9.15% for MCC. These variations in the oxygen content led to variations in O/C ratios.

3.1.3. Surface area

Table 2 displays information on the BET surface area, pore-volume, and pore diameter of carbonaceous materials and magnetic carbonaceous materials. When lignocellulosic biomass goes through a thermochemical process, whether pyrolysis or hydrothermal carbonization, a dehydration reaction occurs, and the release of volatile constituents from the carbon matrix contributes to the formation of the porous structure. As shown in Table 2, CAC possesses a high BET surface area and a high degree of porosity which are 1139.0 m^2 g^{-1} and 0.2402 cm^3 g^{-1}, respectively. In contrast, CC has a low BET surface of about 2.17 m^2 g^{-1}. This difference could be explained because CC is a carbon-based solid obtained by slow pyrolysis by heating wood or vegetable residues without activation. In contrast, CAC is a commercial activated carbon prepared by pyrolysis followed by activation.

Besides, when comparing BC_{SFH} and HC_{SFH} that were prepared using the same feedstock: sunflower husk, however, using two different thermochemical pathways (i.e., the first one by dry pyrolysis (700 °C) and the second one by hydrothermal carbonization (150 °C)), a significant difference in their BET surface area: 493.9 m^2 g^{-1} for BC and 90 m^2 g^{-1} for HC was noticed. These results imply that higher temperatures would contribute to the development of a material with a greater BET surface area. Previous researchers have studied the effect of temperature on the BET surface area and demonstrated that when temperature increases to greatest value, the BET surface area and the porosity increase by promoting the increasing the release of volatile matter [53]. Nevertheless, when it reaches the optimum value, there is a decrease in the BET surface area due to the sintering or collapse of smaller diameter pores. This is consistent with SEM results presented in Fig. 1.

When adding the magnetite nanoparticles into the carbon matrixes, there is a decrease in the BET surface area that could be related to pore blocking, except for MHC_{OR}, where the addition of these magnetic nanoparticles contributed to the increase of the BET surface area changing from 7.8 m^2 g^{-1} in HC_{OR} to 83.5 m^2 g^{-1} in MHC_{OR}. Additionally, all the materials are mesoporous, and the pores have a diameter ranging from 2 to 50 nm.

N_2 adsorption-desorption isotherms of carbonaceous and magnetic carbonaceous material are presented in the supplementary information. Besides, depending on the shape of N_2 adsorption-desorption isotherms, graphs could be classified into VI types. For example, CAC and MAC are type IV characteristics of mesopores. Nevertheless, the initial curvature at lower temperatures indicates the presence of micropores in the sample. On the other hand, CC and MCC are types III and V related to macropores and mesopores. Furthermore, BC_{SFH} and MHC_{SFH} are types I and IV with the presence of micropores and mesopores, respectively. Moreover, HC_{OR} and MHC_{OR} are type III and IV, which means they have macropores and mesopores in their structure.

Table 2
S_{BET}, pore volume, and pore diameter of magnetic and non-magnetic carbonaceous sorbents.

Material	S_{BET} (m^2 g^{-1})	Pore volume (cm^3 g^{-1})	Pore diameter (nm)
CAC	1139.0	0.24022	5.75
CC	2.2	0.00087	4.74
BC_{SFH}	493.9	0.16461	3.01
HC_{OR}	7.8	0.00232	17.39
HC_{SFH}	90.6	0.19000	2.49
MAC	511.4	0.13098	6.44
MCC	57.8	0.00051	11.27
MBC_{SFH}	244.1	0.07466	7.87
MHC_{OR}	83.5	0.08791	5.56
MHC_{SFH}	55.5	0.2360	10.49

3.1.4. FTIR analysis

Fig. 3 shows FTIR spectra of sorbents materials. The band appearing between 3000 and 3500 cm^{-1} is assigned to hydroxyl groups (-OH) stretching mode in all the FTIR spectra. Besides, the band at 1587 cm^{-1} is ascribed to the C═C stretching of the benzene rings. Furthermore, the bands at 1442 and 1368 cm^{-1} are related to the $–CH_2$ scissoring and asymmetric bending vibration, respectively. The typical Fe – O stretching vibration band at 586 cm^{-1} is present in all magnetic carbonaceous materials [54,55]. It could be noticed in the FTIR spectra that when adding magnetite nanoparticles onto the carbon-based matrix, there is a slight shifting in the bands of the magnetic carbonaceous materials, and the intensity fluctuates (especially the O–H and C═C stretching vibration), which suggests there is an interaction between the carbonaceous materials and the magnetite nanoparticles. Jun et al. [49] observed the same behavior where overlapping and shifting of bands of Fe_3O_4 (1035 cm^{-1}) and chars (1605 cm^{-1}) were seen.

3.1.5. Zeta potential

Zeta potential as a function of pH is exhibited in Fig. 4. Zeta potential is the potential that appears between the surface of the sorbent and the medium. As seen in all graphs, the carbonaceous sorbents (CAC, CC, HC_{OR}, HC_{SFH}, BC_{SFH}) depict a negative zeta potential in all pH range

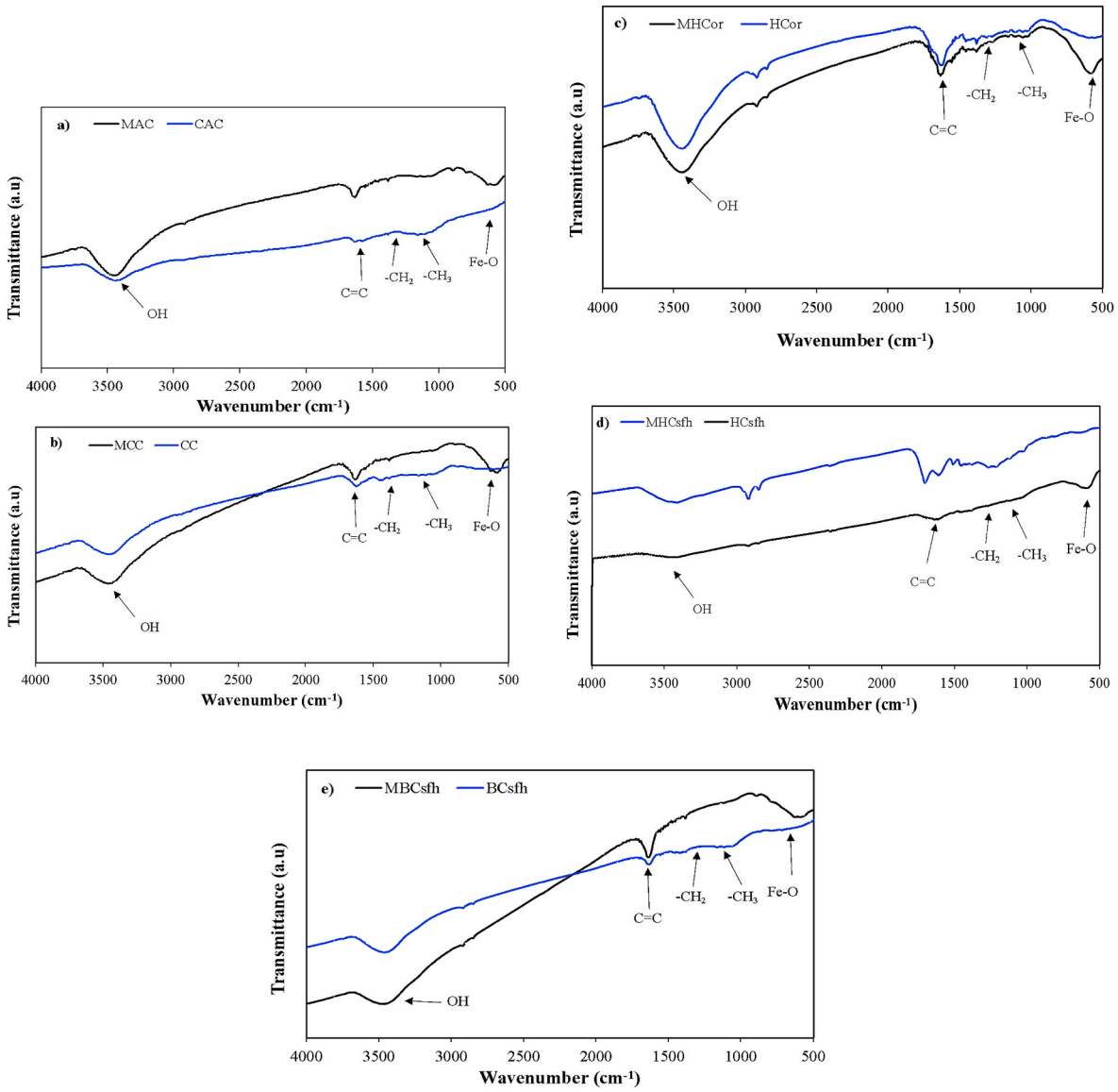

Fig. 3. FTIR of a) CAC and MAC, b) CC and MCC, c) HC_{OR} and MHC_{OR}, d) HC_{SFH} and MHC_{SFH}, and e) BC_{SFH} and MBC_{SFH}.

between 3 and 9, standing out CAC and BC_{SFH} which Z potentials at pH 8.6 and 9.07 are −34.6 and −34.8 mV. In contrast, the magnetic carbonaceous sorbents (MAC, MCC, MHC_{OR}, MBC_{SFH}) possess an isoelectric point (pI) that indicates the pH at which the particles carry no electrical charge [56] at approximately pH 5.2 (MAC), 3.80 (MCC), 3.5 (MHC_{OR}), and 6.5 (MBC_{SFH}). Therefore, above the pH of the isoelectric point, the zeta potential becomes negative, and under the isoelectric point, the zeta potential becomes positive. On the other hand, MHC_{SFH} does not have an isoelectric point.

3.2. Batch sorption kinetics

For kinetics adsorption studies, 250 mg of each sorbent material was put in contact with 250 mL of malachite green solution. During the adsorption studies, various pH values were observed depending on the kind of sorbent employed. This fact was attributable to the release of chemical species, such as organic soluble or inorganic compounds, to the aqueous medium. The initial pH range varies between 2.66 and 6.76 (Table 4). The lowest pH was 2.49 for activated carbon, suggesting that there must be a higher amount of acidic functional groups on its surface, such as carboxylic, lactonic, and phenolic groups; this can be reinforced by the presence of OH vibration at 3500 cm^{-1}, which is a functional groups present in carboxylic and phenolic functional groups [57]. These results suggested that a higher concentration of hydronium ions is released into the aqueous medium due to the dissociation of acidic functional groups when the activated carbon is in contact with water.

On the other hand, MAC possesses the highest pH value of 6.76, which could be related to the fact that when synthesizing the magnetic carbonaceous sorbents, a NaOH solution was used for the magnetic nanoparticle precipitation. It is important to highlight that a purification step was carried out in all the synthesized materials; however, some hydroxyl moieties could have remained as residuals.

Kinetic sorption profiles are presented in Fig. 5a and c. As mentioned, MG was selected as the model organic pollutant to assess its sorption potential using carbonaceous and magnetic carbonaceous materials. It could be noticed that both CAC and MAC have a high sorption capacity removing almost 100% of malachite green within 10 min of contact time. These results could be explained by the large BET surface area of CAC and MAC, that is, the presence of many functional groups presents on the surface could be responsible for the interactions and consequent MB adsorption. Commercial activated carbon is well-known for its sorptive properties attributable to its developed porous structure and

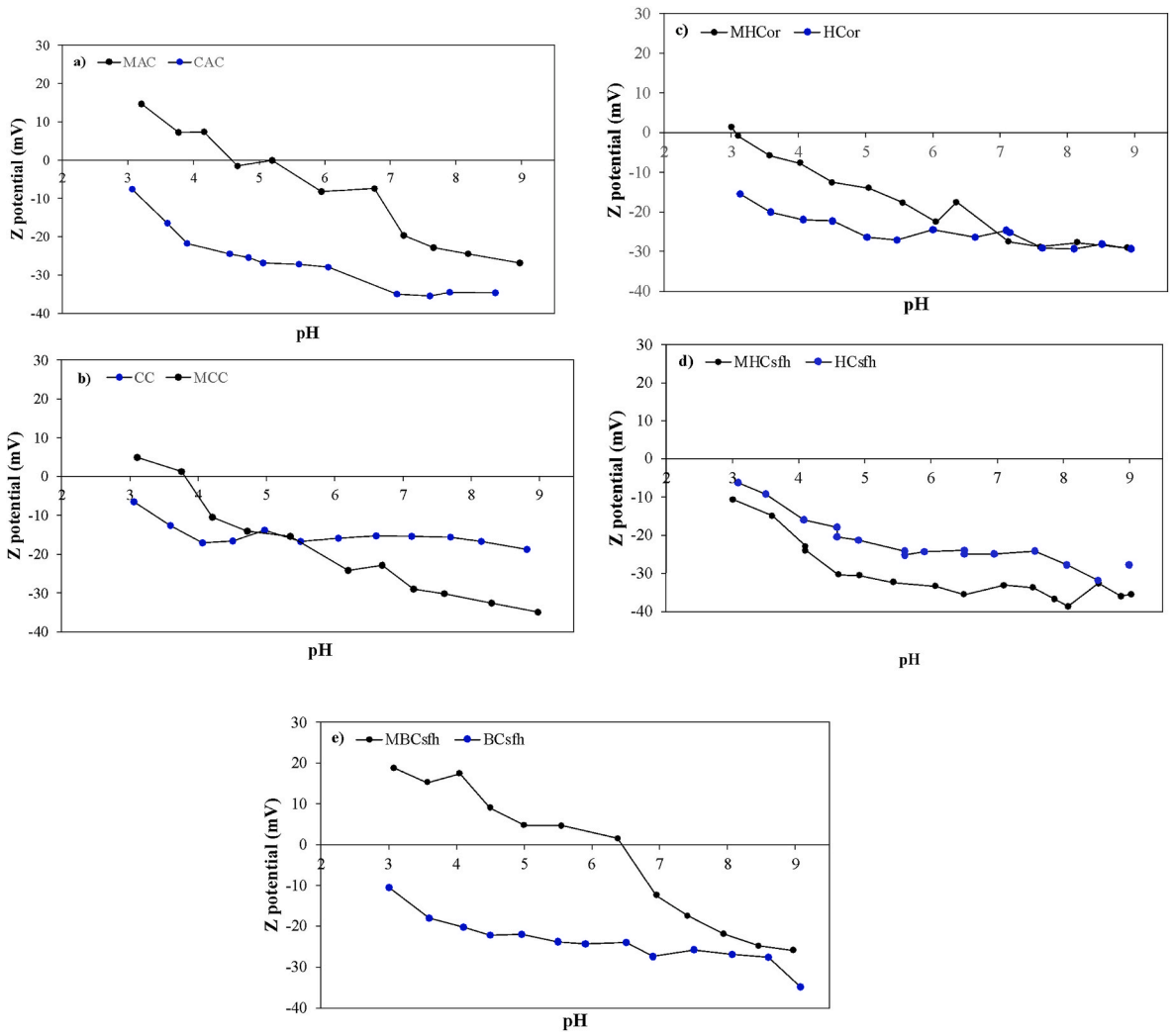

Fig. 4. Z potential as a function of pH of a) CAC and MAC, b) CC and MCC, c) HC_{OR} and MHC_{OR}, d) HC_{SFH} and MHC_{SFH}, and e) BC_{SFH} and MBC_{SFH}.

high surface area [58].

Moreover, it is important to consider the batch pH value as it influences the surface zeta potential and the malachite green chemistry regarding the feasibility of introducing surface interactions with exposed functional groups. As shown in Fig. 5c, MAC has a subtly higher sorption capacity than CAC (Fig. 5a). These results could be explained by the difference in the pH of the batches of MAC and CAC and, subsequently, the Z potential changes. At pH 2.49, CAC tends to be more positive, and at pH 6.76, MAC depicts a negative zeta potential of −7.33 mV. Also, as malachite green pKa is 6.90 [59] and the pH of the batches is under this value, malachite green is in its ionized form, meaning that it is in its cationic form (this could be extrapolated to the behavior of the other sorbents: CC, HC_{SFH}, HC_{OR}, BC_{SFH}, MHC_{SFH}, MHC_{OR}, MBC_{SFH}, and MC). For this reason, MAC interacts stronger by electrostatic interactions with MG than CAC, consequently increasing its removal efficiency.

Nevertheless, the difference in the sorption capacity is not significant since both sorbents reached higher sorption efficiencies. It is crucial to notice that when adding the magnetite nanoparticles into the activated carbon matrix, the BET surface area decreases from 1139.0 to 511.4 m^2 g^{-1}; however, it did not affect the sorption efficiencies of MAC, suggesting that magnetite nanoparticles can be successfully supported on carbonaceous sorbents without affecting their sorption capacities and supplying the carbonaceous sorbents with magnetic properties that are useful when carrying out sorption studies since an external magnetic field might be enough to isolate or concentrate the material as a whole while taking aliquots. Furthermore, the introduction of magnetite nanoparticles into the carbonaceous matrixes could be beneficial for recovering the sorbent material after adsorption and, moreover, leads to an important key, which is reutilization.

In Fig. 5a, the sorbent with the lowest sorption capacities is HC_{OR} reaching the equilibrium at 10.74 mg g^{-1} within 50 min of contact time. Nevertheless, the sorption capacities increased more than twice when adding the magnetite nanoparticles into the HC_{OR} matrix (Fig. 5c), up to 22.39 mg g^{-1} within 50 min of contact time. These results could be explained because magnetite nanoparticles provide the HC_{OR} with more active sites, consistent with the results in section 3.1.2, where the MHC_{OR} BET surface area is higher than HC_{OR}. Additionally, the pH of the batches of HC_{OR} and MHC_{OR} are different: 2.66 and 6.51, respectively. This difference enhances the sorption capacity of the MHC_{OR} due to the sorbent being deprotonated (negative zeta potential of approximately −18 mV), and the dye is in its cationic form, so it promotes the interaction between sorbent and pollutant.

Furthermore, CC and MCC present almost the same behavior from 10 to 120 min of contact time, reaching sorption capacities up to 20.93 and 21.63 mg g^{-1}, respectively. CC and MCC pH are 4.81 and 6.50, respectively, indicating that MCC is more negatively charged, causing an increase in the sorption efficiencies values due to a stronger interaction between MCC and malachite green. Besides, Fig. 5a and c displays the kinetic studies of HC_{SFH} and MHC_{SFH}, where there is a variation in their

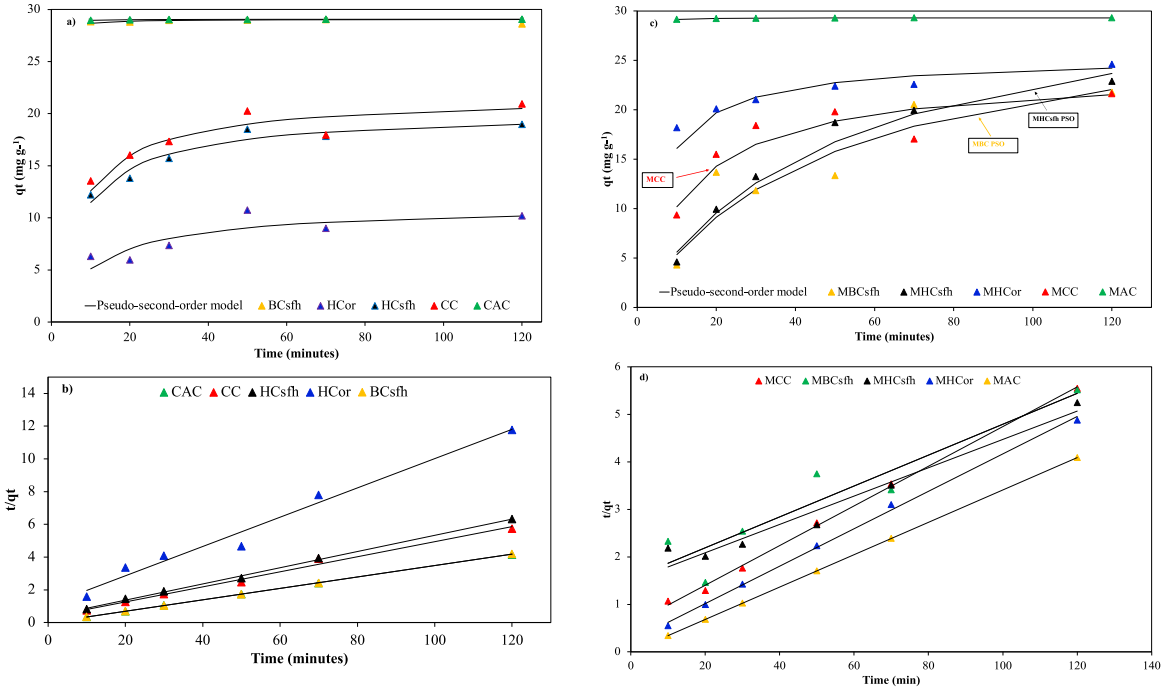

Fig. 5. Plots of a) pseudo-second-order model fitting for MG on carbonaceous sorbents (CAC, CC HC_{SFH}, HC_{OR}, and BC_{SFH}), b) pseudo-second-order model linearization of sorption kinetics of MG on carbonaceous sorbents, c) pseudo-second-order model fitting of MG on magnetic carbonaceous sorbents (MAC, MCC, MHC_{SFH}, MHC_{OR}, and MBC_{SFH}), and d) pseudo-second-order linearization of sorption kinetics of MG on magnetic carbonaceous sorbents. (q_t = adsorption capacity at a time t (mg g^{-1}), t/q_t = linearization of equation (5)).

sorption capacities of 18.98 and 22.87 mg g^{-1} within 120 min of contact time.

3.3. Sorption mechanisms

In Table 3, the kinetic parameters of pseudo-first-order and pseudo-second-order are presented.

Most of the correlation coefficients (R^2) of the pseudo-second-order model are above 0.95 except for MCC and MBC_{SFH}, which are 0.45 and 0.87, respectively (linearization of pseudo-second-order is shown in Fig. 4b–d, and model fitting appears in Fig. 4a–c as a black line). These results show that the experimental sorption capacity is close to the theoretical sorption capacity. However, as seen in Table 3, R^2 of the pseudo-first-order model is far from 1, suggesting that this model does not fit well with experimental data. These results indicate that the pseudo-second-order model describes the kinetics of malachite green sorption onto magnetic and non-magnetic carbonaceous materials [60]. For this reason, as proposed by the pseudo-second-order model, the rate-limiting step of sorption is chemisorption through sharing or exchanging electrons between the sorbents and the malachite green dye.

Table 3
Sorption kinetic parameters of malachite green on carbonaceous and magnetic carbonaceous materials.

Material	PFO			PSO		
	q_e	K_1	R^2	q_e	K_2	R^2
CAC	29.046	0.010	0.103	29.07	0.845	1.00
CC	20.937	0.019	0.594	21.74	0.006	0.990
HC_{SFH}	18.981	0.024	0.692	20.16	0.007	0.998
HC_{OR}	10.740	0.009	0.654	11.17	0.007	0.978
BC_{SFH}	29.030	0.021	0.269	28.65	0.243	1.00
MAC	29.330	0.012	0.558	29.32	0.581	1.00
MCC	21.630	0.013	0.456	3.55	0.003	0.998
MHC_{SFH}	22.870	0.004	0.121	33.55	0.0006	0.959
MHC_{OR}	24.590	0.009	0.633	25.38	0.007	0.997
MBC_{SFH}	21.750	0.025	0.788	30.76	0.0007	0.873

q_e = adsorption capacity at the equilibrium, K_1 = rate constant for the pseudo-first-order model (min^{-1}), K_2 = rate constant for the pseudo-second-order model (g mg^{-1} min^{-1}), R^2 = correlation coefficien

Table 4
Comparative malachite green removal by biochar/agricultural residue/magnetic biochar adsorbent materials in the last years.

Adsorbent	Synthesis methodology	Adsorption capacity (mg g^{-1})	Ref.
EBC (ethanol-biochar from rice husk)	Liquefaction with ethanol at 260 °C	32.5–67.6	56
Oat hulls	Washing and drying at 110 °C, and sieved	83	57
(nZVI/BC) corn straw biochar supported nZVI magnetic	NaOH activation and pyrolysis at 500 °C and magnetite particles by reduction method with $NaBH_4$	515.77	58
(MSBC) magnetic sludge biochar from sewage sludge	assembly of strontium hexaferrite (SrFe12O19) onto SBC under high- temperature and oxygen-free conditions	388.65	59
Magnetic Humic acid	Humic acid activated by K_2CO_3 and precipitation iron oxides onto the activated carbon	476	60
CAC	Pyrolysis and hydrothermal carbonization were used as the thermochemical treatments to transform residues into carbonaceous solids. Following, co-precipitation was employed as magnetite nanoparticles synthesis method. Magnetite nanoparticles were supported on CAC, CC, HC_{SFH}, HC_{OR}, and BC_{SFH}.	29.07	Our work
CC		21.74	
HC_{SFH}		20.16	
HC_{OR}		11.17	
BC_{SFH}		28.65	
MAC		29.32	
MCC		3.55	
MHC_{SFH}		33.55	
MHC_{OR}		25.38	
MBC_{SFH}		30.76	

However, it is highly possible that this was not the only implicated mechanism.

In sorption processes, a combination of different mechanisms usually takes place. As suggested by the kinetic studies included in section 3.2 all the pHs of the batches were under the pKa of malachite green (6.90), indicating that the dye is in its cationic form. Some sorbents possess a negative zeta potential at the batch pH value (CAC, CC, HC_{OR}, HC_{SFH}, BC_{SFH}, MAC, MCC, MHC_{OR}, and MHC_{SFH}) (section 3.1.4). These results indicate that there might also be electrostatic interactions between the cationic and the negatively charged sorbents.

Furthermore, as oxygen-containing functional groups (hydroxyl, carboxyl, and carbonyl, as indicated by FTIR spectra) exist in the sorbents structure, they might promote hydrogen bond interactions with MG. Besides, $\pi - \pi$ interactions are involved since the cationic dye and the sorbents possess cyclic molecules with conjugated carbon-carbon bonds [61]. Also, other van der Waals forces are implicated, such as London dispersion forces that are weak temporary interactions formed by dipoles between the sorbents and MG [62,63]. Finally, some sorbents possess well-defined porous structures (CAC, MAC, MBC_{SFH}, and BC_{SFH}), promoting physical sorption within the pores. For all aforementioned, a combination of different interactions between sorbent materials and malachite green could occur, as represented in Fig. 5d.

3.4. Characterization of post-sorption materials

Fig. 6a–b shows the FTIR spectra of the post-sorption materials. Among all the employed materials in the sorption kinetics, HC_{OR} and MHC_{OR} were designated to be characterized by FTIR due to the significant difference in the adsorption capacity when adding the magnetite nanoparticles into the HC_{OR} matrix. Furthermore, as can be observed in Fig. 6a, there is an evident weakening of the O–H band found between 3000 and 3500 cm^{-1} in the post-sorption materials spectra, which proposes that there might be a strong mechanism of sorption, such as a chemical bond through electron sharing between the nitrogen part of the amine functional group in MG structure and the O–H functional group in the magnetic carbonaceous material. These results are consistent with the results of the fitting to the pseudo-second-order model. Conversely, Fig. 6c exhibits the zeta potential and hydrodynamic diameters of the post-sorption materials are shown in the post-sorption table in Fig. 6. As can be seen, at the corresponding pH, the post-sorption materials acquired more negative zeta potential, from −17.50 mV in the MHC_{OR} initial material to −32.10 mV in the MH_{OR} post-sorption material. These changes indicate that malachite green is bound to carbonaceous materials. Also, hydrodynamic diameters with their corresponding polydispersity index (PDI) of post-sorption materials have decreased, suggesting a better aqueous dispersion. Furthermore, Fig. 6d illustrates the main possible sorption mechanisms involved in removing malachite green (pore filling, electrostatic interactions, electron sharing and π-π interactions).

Table 4 shows the comparative adsorption capacities of different adsorbent materials found in the literature [64–68].

4. Conclusions

Magnetic biochar nanocomposites were prepared by different thermochemical methodologies affecting their chemical structure and elemental composition.

It was observed that of all adsorbents materials employed BC_{SFH}, and MHC_{OR} demonstrated the most capacities for malachite green removal 95.73 and 82.18%, respectively within 120 min of contact time. Furthermore, it was observed that the magnetic carbonaceous sorbents enhance their adsorption capacities when the magnetite nanoparticles were added to the carbon matrixes.

It was demonstrated from the post-adsorption analysis that the mechanisms by which the MB interact with the adsorbents present in this study is a combination of $\pi - \pi$, electrostatic interactions and pore sorption. The present research provides a possible way to reuse biomass wastes by pyrolysis or hydrothermal carbonization and transform them into novel and advanced adsorbent materials with magnetic properties with great potential to eliminate malachite green from water by sorption

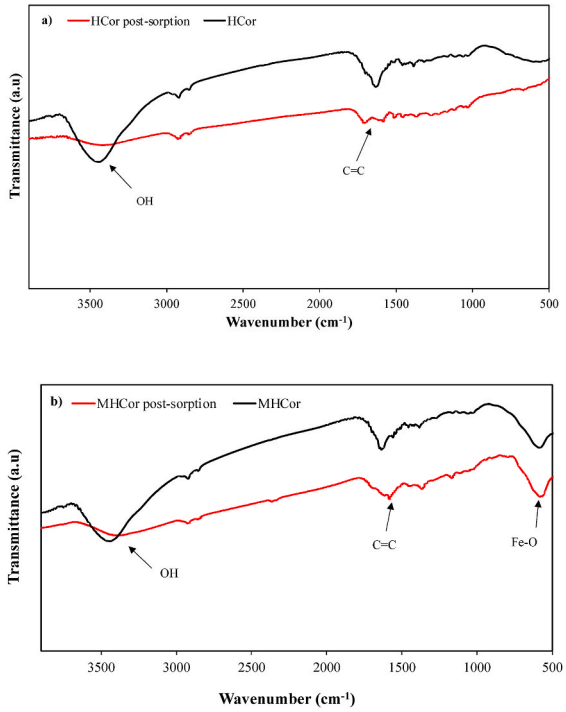

c)

Sample	pH	Zeta potential (mV)	Hydrodynamic diameter (nm)	PDI
HC_{OR}	6.63	-26.4	1223	1
MHC_{OR}	6.31	-17.5	1356	0.71
HC_{OR} post-sorption	6.63	-37.1	728	0.31
MHC_{OR} post-sorption	6.31	-32.1	736	0.49

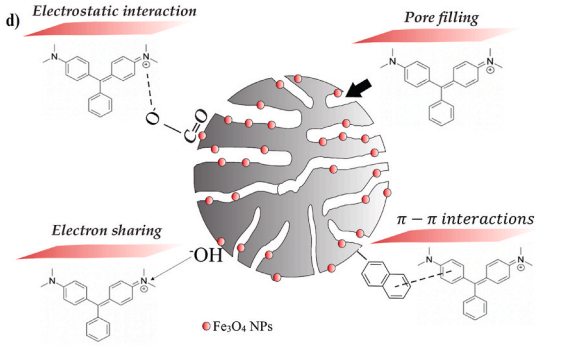

Fig. 6. FTIR spectra of a) H_{OR}, b) MHC_{OR}, c) zeta potential, and hydrodynamic diameters of post-sorption materials, and c) possible mechanisms of green malachite sorption onto magnetic carbonaceous materials. (For interpretation of the references to colour in this figure legend, the reader is referred to the Web version of this article.)

process.

Data availability

Data will be made available on request.

Acknowledgments

This research has been funded by the Ministerio de Ciencia, Innovación y Universidades (MCIU), Agencia Estatal de Investigación (AEI) and Fondo Europeo de Desarrollo Regional (FEDER) of Spain with grant number RTI2018-096695-B-C31; Proyecto de Investigación de Grupos de Investigación (PGI Nº 24/ZQ09 Argentina) and National Research Council Scientific and Technical (CONICET) from Argentina and Minciencias (Ministerio de Ciencia, Tecnología e Investigación de Colombia).

Appendix A. Supplementary data

Supplementary data to this article can be found online at https://doi.org/10.1016/j.biombioe.2023.106772.

References

[1] J. Sharma, S. Sharma, V. Soni, Classification and impact of synthetic textile dyes on aquatic flora: a review, Regional Studies in Marine Science 45 (2021), 101802, https://doi.org/10.1016/j.rsma.2021.101802.
[2] V.K. Garg, R. Kumar, R. Gupta, Removal of malachite green dye from aqueous solution by adsorption using agro-industry waste: a case study of Prosopis cineraria, Dyes Pigments 62 (1) (2004) 1–10, https://doi.org/10.1016/j.dyepig.2003.10.016.
[3] M. Ahmaruzzaman, V.K. Gupta, Rice husk and its ash as low-cost adsorbents in water and wastewater treatment, Ind. Eng. Chem. Res. 50 (24) (2011) 13589–13613, https://doi.org/10.1021/ie201477c.
[4] Y. Al-Degs, M.A.M. Khraisheh, S.J. Allen, M.N. Ahmad, Effect of carbon surface chemistry on the removal of reactive dyes from textile effluent, Water Res. 34 (2000) 3927–3935, https://doi.org/10.1016/S0043-1354(99)00200-6.
[5] M.S.M. Annuar, S. Adnan, S. Vikineswary, Y. Chisti, Kinetics and energetics of azo dye decolorization by Pycnoporus sanguineus, Water, Air, Soil Pollut. 202 (2009) 179–188, https://doi.org/10.1007/s11270-008-9968-5.
[6] R. Katal, H. Zare, S.O. Rastegar, P. Mavaddat, G.N. Darzi, Removal of dye and chemical oxygen demand (COD) reduction from textile industrial wastewater using hybrid bioreactors, Environ. Eng. Manag. J. 13 (1) (2015) 43–50, https://doi.org/10.30638/eemj.2014.007.
[7] I.M. Banat, P. Nigam, D. Singh, R. Marchant, Microbial decolorization of textile-dye-containing effluents: a review, Bioresour. Technol. 58 (3) (1996) 217–227, https://doi.org/10.1016/S0960-8524(96)00113-7.
[8] G. Yin, Z. Sun, Y. Gao, S. Xu, Preparation of expanded graphite for malachite green dye removal from aqueous solution, Microchem. J. 166 (2021), 106190, https://doi.org/10.1016/j.microc.2021.106190.
[9] G.D. Vyavahare, R.G. Gurav, P.P. Jadhav, R.R. Patil, C.B. Aware, J.P. Jadhav, Response surface methodology optimization for sorption of malachite green dye on sugarcane bagasse biochar and evaluating the residual dye for phyto and cytogenotoxicity, Chemosphere 194 (2018) 306–315, https://doi.org/10.1016/j.chemosphere.2017.11.180.
[10] S. Srivastava, R. Sinha, D. Roy, Toxicological effects of malachite green, Aquat. Toxicol. 66 (3) (2004) 319–329, https://doi.org/10.1016/j.aquatox.2003.09.008.
[11] F. Ding, X.N. Li, J.X. Diao, Y. Sun, L. Zhang, L. Ma, X.L. Yang, L. Zhang, Y. Sun, Potential toxicity and affinity of triphenylmethane dye malachite green to lysozyme, Ecotoxicol. Environ. Saf. 78 (2012) 41–49, https://doi.org/10.1016/j.ecoenv.2011.11.006.
[12] E. Sudova1, J. Machova, Z. Svobodova, T. Vesely, Negative effects of malachite green and possibilities of its replacement in the treatment of fish eggs and fish- a review, Vet. Med-US. 52 (12) (2007) 527–539.
[13] S.J. Culp, F.A. Beland, Malachite green: a toxicological review, Int. J. Toxicol. 15 (3) (1996) 219–238, https://doi.org/10.3109/10915819609008715.
[14] A.S. Sartape, A.M. Mandhare, V.V. Jadhav, P.D. Raut, M.A. Anuse, S.S. Kolekar, Removal of malachite green dye from aqueous solution with adsorption technique using Limonia acidissima (wood apple) shell as low cost adsorbent, Arab. J. Chem. 10 (2017) S3229–S3238, https://doi.org/10.1016/j.arabjc.2013.12.019.
[15] B.H. Hameed, M.I. El-Khaiary, Malachite green adsorption by rattan sawdust: isotherm, kinetic and mechanism modeling, J. Hazard Mater. 159 (2008) 574–579, https://doi.org/10.1016/j.jhazmat.2008.02.054.
[16] S. Ayanda, Water treatment technologies: principles, applications, successes and limitations of bioremediation, membrane bioreactor and the advanced oxidation processes, OMICS International (2017), https://doi.org/10.4172/978-1-63278-058-4-059.
[17] J. Lundqvist, A. Andersson, A. Johannisson, E. Lavonen, G. Mandava, H. Kylin, D. Bastviken, Oskarsson, A, Innovative drinking water treatment techniques reduce the disinfection-induced oxidative stress and genotoxic activity, Water Res. 155 (2019) 182–192, https://doi.org/10.1016/j.watres.2019.02.052.
[18] G. Li, H. Yang, T. An, Y. Lu, Antibiotics elimination and risk reduction at two drinking water treatment plants by using different conventional treatment techniques, Ecotoxicol. Environ. Saf. 158 (2018) 154–161, https://doi.org/10.1016/j.ecoenv.2018.04.019.
[19] T.C. Costa, L.T. Hendges, B. Temochko, L.P. Mazur, B.A. Marinho, S. E. Weschenfelder, P.L. Florido, A. da Silva, A.A. Ulson de Souza, S.M.A. Guelli Ulson de Souza, Evaluation of the technical and environmental feasibility of adsorption process to remove water soluble organics from produced water: a review, J. Petrol. Sci. Eng. 208 (2022), 109360, https://doi.org/10.1016/j.petrol.2021.109360.
[20] R. Yousef, H. Qiblawey, M.H. El-Naas, Adsorption as a process for produced water treatment: a review, Processes 8 (12) (2020) 1–22, https://doi.org/10.3390/pr8121657.
[21] M.M. Alam, M.A. Hossain, M.D. Hossain, M.A.H. Johir, J. Hossen, M.S. Rahman, J. L. Zhou, A.T.M.K. Hasan, A.K. Karmakar, M.B. Ahmed, The potentiality of rice husk-derived activated carbon: from synthesis to application, Processes 8 (2) (2020) 203, https://doi.org/10.3390/pr8020203.
[22] M.B. Ahmed, J.L. Zhou, H.H. Ngo, W. Guo, Adsorptive removal of antibiotics from water and wastewater: progress and challenges, Sci. Total Environ. 532 (2015) 112–126, https://doi.org/10.1016/j.scitotenv.2015.05.130.
[23] L. Huang, Y. Sun, W. Wang, Q. Yue, T. Yang, Comparative study on characterization of activated carbons prepared by microwave and conventional heating methods and application in removal of oxytetracycline (OTC), Chem. Eng. J. 171 (3) (2011) 1446–1453, https://doi.org/10.1016/j.cej.2011.05.041.
[24] A.K. Jain, V.K. Gupta, S. Jain, Suhas, Removal of chlorophenols using industrial wastes, Environ. Sci. Technol. 38 (4) (2004) 1195–1200, https://doi.org/10.1021/es034412u.
[25] M. Roosta, M. Ghaedi, A. Daneshfar, R. Sahraei, A. Asghari, Optimization of the ultrasonic assisted removal of methylene blue by gold nanoparticles loaded on activated carbon using experimental design methodology, Ultrason. Sonochem. 1 (2014) 242–252, https://doi.org/10.1016/j.ultsonch.2013.05.014.
[26] Q. Tao, B. Li, Y. Chen, J. Zhao, Q. Li, L. Chen, Q. Peng, S. Yuan, H. Li, R. Huang, C. Wang, An integrated method to produce fermented liquid feed and biologically modified biochar as cadmium adsorbents using corn stalks, Waste Manage. (Tucson, Ariz.) 127 (15) (2021) 112–120, https://doi.org/10.1016/j.wasman.2021.04.027.
[27] Bawaanii Shanmugarajah, Irene MeiLeng Chew, Nabisab Mujawar Mubarak, Thomas SheanYaw Choong, ChangKyoo Yoo, KhangWei Tan, Valorization of palm oil agro-waste into cellulose biosorbents for highly effective textile effluent remediation, J. Clean. Prod. 210 (2019) 697–709, https://doi.org/10.1016/j.jclepro.2018.10.342.
[28] A. Mamaní, N. Ramírez, C. Deiana, M. Giménez, F. Sardella, Highly microporous sorbents from lignocellulosic biomass: different activation routes and their application to dyes adsorption, J. Environ. Chem. Eng. 7 (5) (2019), 103148, https://doi.org/10.1016/j.jece.2019.103148.
[29] J. Grams, Surface analysis of solid products of thermal treatment of lignocellulosic biomass, J. Anal. Appl. Pyrolysis 161 (2022), 105429, https://doi.org/10.1016/j.jaap.2021.105429.
[30] S. Shyam, J. Arun, K.P. Gopinath, G. Ribhu, M. Ashish, S. Ajay, Biomass as source for hydrochar and biochar production to recover phosphates from wastewater: a review on challenges, commercialization, and future perspectives, Chemosphere 286 (2022), 131490, https://doi.org/10.1016/j.chemosphere.2021.131490.
[31] Y. Xie, L. Wang, H. Li, L.J. Westholm, L. Carvalho, E. Thorin, Z. Yu, X. Yu, O. Skreiberg, A critical review on production, modification and utilization of biochar, J. Anal. Appl. Pyrolysis 161 (2022), 105405, https://doi.org/10.1016/j.jaap.2021.105405.
[32] S. Xu, J. Chen, H. Peng, S. Leng, H. Li, W. Qu, Y. Hu, H. Li, S. Jiang, W. Zhou, L. Leng, Effect of biomass type and pyrolysis temperature on nitrogen in biochar, and the comparison with hydrochar, Fuel 291 (2021), 120128, https://doi.org/10.1016/j.fuel.2021.120128.
[33] C.G. Castro, A.H. Trevisan, D.C.A. Pigosso, J. Mascarenhas, The rebound effect of circular economy: definitions, mechanisms and a research agenda, J. Clean. Prod. 345 (2022), 131136, https://doi.org/10.1016/j.jclepro.2022.131136.
[34] C.Y. Tsai, P.Y. Lin, S.L. Hsieh, R. Kirankumar, A.K. Patel, R.R. Singhania, C. di Dong, C.W. Chen, S. Hsieh, Engineered mesoporous biochar derived from rice husk for efficient removal of malachite green from wastewaters, Bioresour. Technol. 347 (2022), 126749, https://doi.org/10.1016/j.biortech.2022.126749.
[35] L. Leng, X. Yuan, G. Zeng, J. Shao, X. Chen, Z. Wu, H. Wang, X. Peng, Surface characterization of rice husk bio-char produced by liquefaction and application for cationic dye (Malachite green) adsorption, Fuel 155 (2015) 77–85, https://doi.org/10.1016/j.fuel.2015.04.019.
[36] A.A.B. Patiño, V.L. Lassalle, M.F. Horst, Magnetic hydrochar nanocomposite obtained from sunflower husk: a potential material for environmental remediation, J. Mol. Struct. 1239 (2021), https://doi.org/10.1016/j.molstruc.2021.130509.
[37] J. Qu, S. Wang, L. Jin, Y. Liu, R. Yin, Z. Jiang, Y. Tao, J. Huang, Y. Zhang, Magnetic porous biochar with high specific surface area derived from microwave-assisted hydrothermal and pyrolysis treatments of water hyacinth for Cr(VI) and tetracycline adsorption from water, Bioresour. Technol. 340 (2021), 125692, https://doi.org/10.1016/j.biortech.2021.125692.
[38] C. Wurzer, O. Mašek, Feedstock doping using iron rich waste increases the pyrolysis gas yield and adsorption performance of magnetic biochar for emerging contaminants, Bioresour. Technol. 321 (2021), 124473, https://doi.org/10.1016/j.biortech.2020.124473.

[39] Y. Chen, F. Xu, H. Li, Y. Li, Y. Liu, Y. Chen, M. Li, L. Li, H. Jiang, L. Chen, Simple hydrothermal synthesis of magnetic MnFe2O4-sludge biochar composites for removal of aqueous Pb2+, J. Anal. Appl. Pyrolysis 156 (2021), 105173 https://doi.org/10.1016/j.jaap.2021.105173.

[40] M.T.H. Siddiqui, Humair Ahmed Baloch, Sabzoi Nizamuddin, N.M. Mubarak, Shaukat Ali Mazari, G.J. Griffin, Madapusi Srinivasan, Dual-application of novel magnetic carbon nanocomposites as catalytic liquefaction for bio-oil synthesis and multi-heavy metal adsorption, Renew. Energy 172 (2021) 1103–1119, https://doi.org/10.1016/j.renene.2021.02.157.

[41] Y. Yi, G. Tu, G. Ying, Z. Fang, E.P. Tsang, Magnetic biochar derived from rice straw and stainless steel pickling waste liquor for highly efficient adsorption of crystal violet, Bioresour. Technol. 341 (2021), 125743, https://doi.org/10.1016/j.biortech.2021.125743.

[42] N.M. Mubarak, R.F. Alicia, E.C. Abdullah, J.N. Sahu, A.B. Ayu Haslija, J. Tan, Statistical optimization and kinetic studies on removal of Zn2+ using functionalized carbon nanotubes and magnetic biochar, J. Environ. Chem. Eng. 1 (3) (2013) 486–495, https://doi.org/10.1016/j.jece.2013.06.011.

[43] F. Huang, S.M. Zhang, R.R. Wu, L. Zhang, P. Wang, R.B. Xiao, Magnetic biochars have lower adsorption but higher separation effectiveness for Cd2+ from aqueous solution compared to nonmagnetic biochars, Environ. Pollut. 275 (2021), 116485, https://doi.org/10.1016/j.envpol.2021.116485.

[44] N.M. Mubarak, A. Kundu, J.N. Sahu, E.C. Abdullah, N.S. Jayakumar, Synthesis of palm oil empty fruit bunch magnetic pyrolytic char impregnating with FeCl3 by microwave heating technique, Biomass Bioenergy 61 (2014) 265–275, https://doi.org/10.1016/j.biombioe.2013.12.021.

[45] A.A. Burbano, G.A. Muñoz Medina, F.H. Sánchez, V.L. Lassalle, M.F. Horst, G. Gascó, A. Méndez, Catalytic Activity of Carbon Materials in the Oxidation of Minerals, Biomass Conversion and Biorefinery, 2022, https://doi.org/10.1007/s13399-022-03517-7.

[46] M.F. Horst, D.F. Coral, M.B. Fernández van Raap, et al., Hybrid nanomaterials based on gum Arabic and magnetite for hyperthermia treatments, Mater. Sci. Eng. C 74 (2016) 443–450, https://doi.org/10.1016/j. msec.2016.12.035.

[47] C. Santhosh, E. Daneshvar, K.M. Tripathi, P. Baltrėnas, T.Y. Kim, E. Baltrėnaitė, A. Bhatnagar, Synthesis and characterization of magnetic biochar adsorbents for the removal of Cr(VI) and Acid orange 7 dye from aqueous solution, Environ. Sci. Pollut. Res. 27 (2020) 32874–32887, https://doi.org/10.1007/s11356-020-09275-1.

[48] M. Kwiatkowski, D. Kalderis, A complementary analysis of the porous structure of biochars obtained from biomass, Carbon Lett 30 (3) (2020) 325–329, https://doi.org/10.1007/s42823-019-00101-4.

[49] A. Dieguez-Alonso, A. Funke, A. Anca-Couce, A.G. Rombolà, G. Ojeda, J. Bachmann, F. Behrendt, Towards biochar and hydrochar engineering-influence of process conditions on surface physical and chemical properties, thermal stability, nutrient availability, toxicity and wettability, Energies 11 (3) (2018) 496, https://doi.org/10.3390/en11030496.

[50] H.S. Kambo, A. Dutta, A comparative review of biochar and hydrochar in terms of production, physico-chemical properties, and applications, Renew. Sustain. Energy Rev. 45 (2015) 359–378, https://doi.org/10.1016/j.rser.2015.01.050.

[51] C.A. Takaya, L.A. Fletcher, S. Singh, K.U. Anyikude, A.B. Ross, Phosphate and ammonium sorption capacity of biochar and hydrochar from different wastes, Chemosphere 145 (2016) 518–527, https://doi.org/10.1016/j.chemosphere.2015.11.052.

[52] W. Vercruysse, J. Smeets, T. Haeldermans, B. Joos, A. Hardy, P. Samyn, J. Yperman, K. Vanreppelen, R. Carleer, P. Adriaensens, W. Marchal, D. Vandamme, Biochar from raw and spent common ivy: impact of preprocessing and pyrolysis temperature on biochar properties, J. Anal. Appl. Pyrolysis 159 (2021), 105294, https://doi.org/10.1016/j.jaap.2021.105294.

[53] S. Rodríguez-Sánchez, B. Ruiz, D. Martínez-Blanco, M. Sánchez-Arenillas, M. A. Diez, J.F. Marco, P. Gorria, E. Fuente, Towards advanced industrial waste-based magnetic activated carbons with tunable chemical, textural and magnetic properties, Appl. Surf. Sci. 551 (2021), 149407, https://doi.org/10.1016/j.apsusc.2021.149407.

[54] M. Stoia, R. Istratie, C. Păcurariu, Investigation of magnetite nanoparticles stability in air by thermal analysis and FTIR spectroscopy, J. Therm. Anal. Calorim. 125 (2016) 1185–1198, https://doi.org/10.1007/s10973-016-5393-y.

[55] B.M. Jun, Y. Kim, J. Han, Y. Yoon, J. Kim, C.M. Park, Preparation of activated biochar-supported magnetite composite for adsorption of polychlorinated phenols from aqueous solutions, Water 11 (9) (2019) 1899, https://doi.org/10.3390/w11091899.

[56] M.S. Alam, B. Bishop, N. Chen, S. Safari, V. Warter, J.M. Byrne, T. Warchola, A. Kappler, K.O. Konhauser, D.S. Alessi, Reusable magnetite nanoparticles–biochar composites for the efficient removal of chromate from water, Sci. Rep. 10 (1) (2020), 19007, https://doi.org/10.1038/s41598-020-75924-7.

[57] A.S. Da Costa Lopes, S.M.L. de Carvalho, D. do Socorro Barros Brasil, R. de Alcântara Mendes, M.O. Lima, Surface modification of commercial activated carbon (CAG) for the adsorption of benzene and toluene, Am. J. Anal. Chem. 6 (2015) 528–538, https://doi.org/10.4236/ajac.2015.66051.

[58] B. Xie, J. Qin, S. Wang, X. Li, H. Sun, W. Chen, Adsorption of phenol on commercial activated carbons: modelling and interpretation, Int. J. Environ. Res. Publ. Health 17 (3) (2020) 789, https://doi.org/10.3390/ijerph17030789, 28.

[59] V.M. Muinde, J.M. Onyari, B. Wamalwa, J.N. Wabomba, Adsorption of malachite green dye from aqueous solutions using mesoporous chitosan–zinc oxide composite material, Environ. Toxicol. Chem. 2 (2020) 115–125, https://doi.org/10.1016/j.enceco.2020.07.005.

[60] E. Bulut, M. Özacar, I.A. Şengil, Adsorption of malachite green onto bentonite: equilibrium and kinetic studies and process design, Microporous Mesoporous Mater. 115 (2008) 234–246, https://doi.org/10.1016/j.micromeso.2008.01.039.

[61] Hai Nguyen Tran, Ya-Fen Wang, Sheng-Jie You, Huan-Ping Chao, Insights into the mechanism of cationic dye adsorption on activated charcoal: the importance of – interactions, Process Saf. Environ. Protect. 107 (2017) 168–180, https://doi.org/10.1016/j.psep.2017.02.010.

[62] A.A. Ahmad, M.A. Ahmad, N.K.E.M. Yahaya, J. Karim, Adsorption of malachite green by activated carbon derived from gasified Hevea brasiliensis root, Arab. J. Chem. 14 (4) (2021), 103104, https://doi.org/10.1016/j.arabjc.2021.103104.

[63] T.G. Ambaye, M. Vaccari, E.D. Van Hullebusch, A. Amrane, S. Rtimi, Mechanisms and adsorption capacities of biochar for the removal of organic and inorganic pollutants from industrial wastewater, Int. J. Environ. Sci. Technol. 18 (2021) 3273–3294, https://doi.org/10.1007/s13762-020-03060-w.

[64] Lijian Leng, Xingzhong Yuan, Guangming Zeng, Jianguang Shao, Xiaohong Chen, Zhibin Wua, Hou Wang, Xin Peng, Surface characterization of rice husk bio-char produced by liquefaction and application for cationic dye (Malachite green) adsorption, Fuel 155 (2015) 77–85, https://doi.org/10.1016/j.fuel.2015.04.019.

[65] Gopesh C. Sharma, Ravindra Kumar Gautam, M.C. Chattopadhyaya, Siddh N. Upadhyay, Yogesh Chandra Sharma, Removal of Malachite Green, a hazardous dye from aqueous solutions using Avena sativa (oat) hull as a potential adsorbent, J. Mol. Liq. 213 (2016) 162–172, https://doi.org/10.1016/j.molliq.2015.11.011.

[66] A.S. Eltaweil, H. Ali Mohamed, Eman M. Abd El-Monaem, G.M. El-Subruiti, Mesoporous magnetic biochar composite for enhanced adsorption of malachite green dye: characterization, adsorption kinetics, thermodynamics, and isotherms, Adv. Powder Technol. 31 (3) (2020) 1253–1263, https://doi.org/10.1016/j.apt.2020.01.005.

[67] Jing Zhang, Mao Liu, Tao Yang, Kai Yang, Hongyu Wang, A novel magnetic biochar from sewage sludge: synthesis and its application for the removal of malachite green from wastewater, Water Sci. Technol. 74 (8) (2016) 1971–1979, https://doi.org/10.2166/wst.2016.386.

[68] Xiangdong Zhu, Yuchen Liu, Chao Zhou, Shicheng Zhang, Jianmin Chen, Novel and high-performance magnetic carbon composite prepared from waste hydrochar for dye removal, ACS Sustain. Chem. Eng. 2 (4) (2014) 969–977, https://doi.org/10.1021/sc400547y.